
Cox, Peter M.; Pearson, David; Booth, Ben B.; Friedlingstein, Pierre; Huntingford, Chris; Jones, Chris D.; Luke, Catherine M.. 2013. **Sensitivity of tropical carbon to climate change constrained by carbon dioxide variability.** *Nature*, 494 (7437). 341-344. https://doi.org/10.1038/nature11882

Sensitivity of tropical carbon to climate change constrained by carbon dioxide variability

Peter M. Cox[1], David Pearson[2],

Ben B. Booth[2], Pierre Friedlingstein[1], Chris Huntingford[3], Chris D. Jones[2], Catherine M. Luke[1]

[1] *College of Engineering, Mathematics and Physical Science, University of Exeter, EX4 4QF, UK*

[2] *Hadley Centre, Met Office, Exeter, EX1 3PB, UK*

[3] *Centre for Ecology and Hydrology, Wallingford, Oxon OX10 8BB, UK*

The response of tropical forests to climate change is a key unknown in climate projections for the 21st Century[1,2]. Coupled climate-carbon cycle models generally agree that carbon storage on land will increase as a result of direct CO_2 effects on plant photosynthesis and water-use efficiency, but decrease due to climate change[3]. The balance between these effects varies markedly between models, leading to a range in projected change in carbon stored on tropical land of 330GtC by 2100. Explanations for this large uncertainty, range from differences in the predicted change in rainfall in Amazonia[4,5], to variation in the responses of alternative vegetation models to warming[6]. Here we identify an emergent linear relationship across the ensemble of models[7] between the sensitivity of tropical land-carbon storage to warming and the sensitivity of the annual growth-rate in atmospheric CO_2 to tropical temperature anomaliess[8]. Combined with contemporary observations of atmospheric CO_2 concentration and tropical temperature, this relationship provides a tight constraint on the sensitivity of tropical land carbon to climate change. We estimate a loss of tropical land carbon of 53+/-17 GtC per Kelvin of warming in the tropics (30^{o}N-30^{o}S). Compared to the unconstrained ensemble of climate-carbon cycle projections, this indicates a much lower risk of Amazon forest dieback under CO_2-induced climate[9]. However with no balancing CO_2-fertilisation, this gives greater certainty that carbon would be lost from the tropical land under warming associated with non-CO_2 climate forcing factors[10,11].

We utilise results from the Coupled Climate-Carbon Cycle Model Intercomparison Project[3] (C^4MIP) focussing on changes in tropical land carbon storage in the latitudinal band from 30^{o}N to 30^{o}S. Although C^4MIP included General Circulation Models (GCMs) and Earth System Models of Intermediate Complexity (EMICS), we limit our analysis to the GCMs since our emergent constraint requires models that generate interannual variability. The C^4MIP experimental design[3] forced models by the SRES A2 scenario[12] of anthropogenic CO_2 emissions (including those due to land-use change). For each model an "uncoupled" simulation was carried-out in which the land and ocean carbon cycles were made insensitive to the climate change caused by the increase in atmospheric CO_2. Comparison between the coupled and uncoupled simulations allows the direct impacts of CO_2 on land and ocean carbon sinks to be separated from the impacts of climate change[3,13]. We test the emergent constraint derived from the C_4MIP GCMs against results from the recent HadCM3 land carbon cycle ensemble[14].

Our emergent constraint could also be tested against the recent CMIP5 climate-carbon cycle models, which will appear in the IPCC 5th Assessment Report (AR5), However, the AR5 models typically use prescribed concentrations of atmospheric CO_2[15]. This makes direct comparison to the observed interannual variability in the atmospheric CO_2 concentration difficult. As such, the emergent constraint we present here is conditional on the simplistic representations of the carbon cycle in the C_4MIP models.

Table 1 summarises results from six C_4MIP GCMs (A to F; Table 1) for 1960 to 2099. For all models the impact of climate change on the carbon cycle results in a larger increase in atmospheric CO_2 in the coupled versus uncoupled simulation. This amplification varies by an order of magnitude across the model ensemble (from an extra 18ppmv in model D to an extra 212ppmv in model A). A large part of this uncertainty arises from differing responses of tropical land carbon to projected climate changes in each model. All models produce a significant increase in tropical land carbon storage in the uncoupled simulations due to the direct effects of CO_2 on photosynthesis and water-use efficiency (+263 GtC in model F to +413 GtC in model C). The neglect of carbon-nitrogen interactions in this first generation of climate-carbon models is arguably a major limitation in the mid and high-latitudes[16], but is much less problematic in tropical forests which are not typically nitrogen-limited[17]. Forest inventories are also consistent with a significant CO_2 fertilization in the tropics[18,19]. Despite the reasonable agreement amongst models on the impact of CO_2 fertilization, the fully coupled simulations produce very different changes in tropical land carbon storage from 1960 to 2099 (-11 GtC for model A to +319 GtC for model D). .

Figure 1(a) represents the evolution of tropical land carbon storage in the C_4MIP models, with the upper and lower estimates shown for both the coupled and uncoupled simulations. The lower estimate in the coupled simulation comes from the HadCM3LC model that projects Amazon forest dieback under CO_2 induced climate change[1,9,10]. In this model tropical land carbon storage increases due to direct CO_2 effects until around 2050, but then declines abruptly due to warming and drying in Amazonia[9]. This projection, along with recent extreme droughts in Amazonia[20,21,22], suggests tropical forest dieback could be a high-impact tipping element in the Earth's climate system[23].

To separate direct impacts of CO_2 from impacts of climate change, we follow previous analyses[3,13] in writing the change in tropical land carbon storage, ΔC_{LT}, in terms of the change in atmospheric CO_2, ΔC_a, and the change in tropical mean temperature, ΔT_T:

$$\Delta C_{LT} = \beta_{LT}\, \Delta C_a + \gamma_{LT}\, \Delta T_T$$

where β_{LT} (GtC/ppmv) and γ_{LT} (GtC/K) are the sensitivity of tropical land carbon storage to direct CO_2 effects and climate change respectively. The uncoupled simulations are used to estimate β_{LT} for each model, and then these values are used to isolate γ_{LT} from the coupled simulations[3,13] by subtracting off the direct CO_2 effect. Figure 1(b) is a scatter plot of $\{\beta_{LT}, \gamma_{LT}\}$ for each C4MIP model and the three HadCM3 ensemble members. Whereas the β_{LT} values span a factor of two from about 0.5 to 1 GtC/ppmv, the γ_{LT} values range over a factor of more than four from -29 GtC/K (model F) to -133 GtC/K (model A), with a C4MIP mean of -69 GtC/K and a standard deviation of 39 GtC/K. This range is even larger if the HadCM3 ensemble members are included. We therefore focus on reducing the larger uncertainty in γ_{LT}.

Our inspiration for deriving a multi-model emergent constraint comes from a recent study which showed a strong relationship between the contemporary temperature sensitivity of seasonal snow-cover and the magnitude of the snow-albedo feedback, across more than twenty GCMs[7]. Since the seasonal cycle of snow-cover can be estimated from observations, this model-derived relationship converts the contemporary observations to a constraint on the size of the snow-albedo feedback in the real climate system, for which there is no direct reliable measurement. Emergent constraints of this type utilise the often bewildering spread amongst Earth System model projections to reduce uncertainties in the sensitivities of the real Earth System to anthropogenic forcing. They are distinct and complementary to bottom-up constraints arising from process-based studies.

It made sense *a priori* to look for an emergent constraint linking the sensitivity of tropical land carbon to interannual variability (IAV) in the growth-rate of atmospheric CO_2. Tropical land carbon changes in response to climate through changes in the net land-atmosphere CO_2 flux moving in and out of this carbon store. Critically, the sensitivity of this net tropical CO_2 flux is revealed by the IAV of the CO_2 growth-rate, as this is known to be dominated by the response of the tropical land carbon cycle to climatic anomalies (Supplementary Material, Figure S1a) such as the El Nino Southern Oscillation[8,24,25]. Hence, some relationship between IAV of CO_2 and the longer-term sensitivity of tropical land carbon storage to climate change (γ_{LT}) is to be expected, so long as processes which are not evident in the short-term variation of the CO_2 fluxes (e.g. forest dynamics or changes in long-lived soil carbon pools) do not dominate the long-term response. This is our working hypothesis to be tested against the C4MIP models which include a range of representations of slow vegetation and soil processes[3].

Figure 2(a) compares the observed IAV of the growth-rate of global atmospheric CO_2[26,27] to the IAV of the annual mean tropical temperature[28]. In both cases we have chosen observational variables (global mean atmospheric CO_2 and mean land plus ocean temperature between 30^oN and 30^oS) for consistency with the variables available from the C4MIP models. Aside from the years immediately after the volcanic eruptions[24] of Mt Agung, El Chichon, and Pinatubo, IAV in the growth-rate of atmospheric CO_2 is linearly correlated with the IAV of the tropical temperature ($r=0.65$, $p<0.0001$) (Figure 2b), with a best-fit "IAV sensitivity" of 5.1+/-0.9 GtC/yr/K. Excluding these volcano-affected years has a less than 5% impact on the best-fit sensitivity, but avoids the complication of diffuse-light fertilization of plant growth[29] which is not included in any of the C4MIP models.We also find a similar sensitivity regardless of which tropical temperature reconstruction we use. There is a greater sensitivity to the choice of the global atmospheric CO_2 dataset, but this does not affect our overall conclusions (Supplementary Material, Table S1).

A similar calculation is made for each of the coupled climate-carbon cycle models, to derive the sensitivity of the CO_2 growth-rate to tropical temperature for the period 1960-2010. Compared to the observational data, models tend to overestimate the IAV of the tropical temperature by up to a factor of two, and overestimate the IAV of the CO_2 growth-rate by up to a factor of three. The correlation between these variables is underestimated in some models (model F, B and D) and over-estimated in others (model A, E and C). Hence, IAV sensitivity varies across the C4MIP model ensemble from 2.9+/-1.4 GtC/yr/K (model F) to 9.7+/-0.7 GtC/yr/K (model A), with most of this range being due to differences in the sensitivity of heterotrophic respiration to climate (see Supplementary Material, Figure S1b). The three HadCM3 ensemble members, which were produced by perturbing only parameters in the land carbon cycle component of the model[13], span an even larger range (5.6 to 14.4 GtC/yr/K) - suggesting that uncertainties in the modelling of the tropical land carbon cycle are critical.

Most importantly, these differing IAV sensitivities are strongly-correlated ($r=0.98$, $p=0.0005$) with variations in γ_{LT} across C4MIP models (black letters; Figure 3(a)). The dashed red line in Figure 3(a) shows the best-fit straight-line relating these variables for the six C4MIP GCMs (although in principle a well-defined non-linear function would also yield an emergent constraint). Red letters in Figure 3(a) show how well this relationship would have predicted the variation in γ_{LT} for the three HadCM3 ensemble members given the IAV sensitivity of each. Note that two of the HadCM3 variants have γ_{LT} values beyond the range of the C4MIP models, and yet the extrapolated straight-line is able to fit these outliers. The dotted vertical black lines in Figure 3(a) show the IAV sensitivity (plus and minus one standard deviation), as previously estimated from the contemporary observations, from which we derive tighter bounds on γ_{LT}.

With the model-derived relationship between γ_{LT} and the IAV sensitivity, we can use the observational constraint to estimate a probability density function (PDF) for γ_{LT} (Methods). Figure 3(b) compares this to the PDF arising from assuming all C4MIP models are equally likely to be true and come from an underlying Gaussian distribution (red line). The emergent constraint from the IAV sensitivity of the CO_2 growth-rate sharpens the PDF of γ_{LT} and moves its peak to a less negative value (53+/-17 as opposed to 69 +/-39 GtC/yr/K). The application of the IAV constraint reduces the estimated probability of γ_{LT} values more negative than -100 GtC/K, typically associated with models that project CO_2-induced tropical forest dieback, by almost two orders of magnitude from 21% to 0.24%.

The IAV constraint also implies greater confidence that tropical land carbon is vulnerable to warming caused by non-CO_2 forcing factors[11]. Remaining uncertainties for tropical land climate-carbon cycle feedbacks are therefore the magnitude of long-term CO_2-fertilization effects in the tropics, and the extent to which future climate change will be caused by non-CO_2 factors.

Methods Summary

We used results from six of the eleven models that took part in the Coupled Climate-Carbon Cycle Model Intercomparison Project (C4MIP)[3]. The excluded five models consisted of four Earth System Models of Intermediate Complexity (EMICs) – which do not typically generate internal variability as required to define the interannual sensitivity of the CO_2 growth-rate to tropical temperature anomalies, and one GCM (LLNL) - which reported zonal mean land temperatures rather than zonal mean (land and ocean) temperatures. Outputs from the remaining six models were reported as annual means for each 30^o latitudinal band (available via:

https://c4mip.lsce.ipsl.fr/diagnostics_phase2.html). We combined the outputs from the 30°N-0°N and 0°S-30°S bands to define the projected changes for the 30°N-30°S "tropical" band.

Models G, H and I in this study, which are used to test the emergent constraint derived from the C4MIP models, come from a land carbon cycle ensemble carried out with the HadCM3C model[14]. HadCM3C is similar to C4MIP model A (HadCM3LC) but includes a higher resolution ocean model (1.25° x 1.25° rather than 2.5° x 3.75°) and also interactive atmospheric sulphur cycle chemistry. Seventeen HadCM3C ensemble members were defined by perturbations to key land-surface parameters including leaf nitrogen concentrations and the temperature sensitivities of photosynthesis and soil respiration[14]. All ensemble members were driven by the SRES A1B emissions scenarios, including changes in non-CO_2 forcing factors (most notably changes in anthropogenic sulphate aerosols[10]). Uncoupled simulations were only carried-out for the standard parameter values (HadCM3-st), and the ensembles members leading to the lowest (HadCM3-a) and highest (HadCM3-h) global carbon cycle feedbacks. We therefore focussed on these three variants of HadCM3C for this study.

The analysis of the model outputs and observational data, and the statistical methods employed are outlined in the online "Methods".

References

1. Cox, P.M., Betts, R.A., Jones, C.D., Spall, S.A. & Totterdell, I.J.. Acceleration of global warming due to carbon cycle feedbacks in a coupled climate model. *Nature*, **408**, 184-187 (2000).
2. Malhi, Y., *et al*. Climate change, deforestation, and the fate of the Amazon. *Science*, 319, 169-172 (2008).
3. Friedlingstein, P. *et al.* Climate-carbon cycle feedback analysis: Results from the C4MIP model intercomparison. *J. Climate*, **19**, 3337-3353 (2006).
4. Jupp, T.E., *et al*. Development of probability density functions for future Amazonian rainfall. *New Phytologist*, **18**, 682-693 (2010).
5. Rammig, A., *et al*. Estimating the risk of Amazonian forest dieback. *New Phytologist*, **187**, 694-706 (2010). Galbraith, D., *et al*.
6. Galbraith, D., *et al*. Multiple mechanisms of Amazonian forest biomass losses in three dynamic global vegetation models under climate change. *New Phytologist*, **187**, 647-665 (2010).
7. Hall, A. and Qu, X. Using the current seasonal cycle to constrain snow albedo feedback in future climate change. *Geophysical Research Letters*, **33**, L03502 (2006).
8. Bacastow, R.. Modulation of atmospheric carbon dioxide by the Southern Oscillation. *Nature*, **261**, 116-118 (1976).

9. Cox, P.M. *et al*. Amazon dieback under climate-carbon cycle projections for the 21st century. *Theoretical and Applied Climatology*, **78**, 137-156 (2004).
10. Cox, P.M., *et al*. Increasing risk of Amazonian drought due to decreasing aerosol pollution. *Nature*, **453**, 212-216 (2008).
11. Huntingford, C., *et al*. Highly contrasting effects of different climate forcing agents on ecosystem services. Phil. Trans. Roy. Soc. A., **369**, 2026-2037 (2011).
12. Nakicenovic, N. *et al.*. *Special Report on Emissions Scenarios, Summary for Policy Makers*, Intergovernmental Panel on Climate Change, Geneva, Switzerland (2000).
13. Friedlingstein, P., Defresne J.-L., Cox P.M. & Rayner P. How positive is the feedback between climate change and the carbon cycle? *Tellus* , **55B** , 692-700 (2003).
14. Booth, B.B.B., *et al.* High sensitivity of future global warming to land carbon cycle processes. *Environmental Research Letters (in press).*
15. Moss, R.H., *et al.* The next generation of scenarios for climate change research and assessment. *Nature,* 463, 747-756 (2010).
16. Hungate, B.A., *et al*. Nitrogen and climate change. *Science*, 302, 1512-1513 (2003).
17. Zaehle, S., Friedlingstein, P. & Friend, A.D. Terrestrial nitrogen feedbacks may accelerate future climate change. *Geophysical Research Letters*, **37**, L01401 (2010).
18. Baker, T.R., *et al*. Increasing biomass in Amazonian forest plots. *Phil. Trans. Roy. Soc. B*, **359**, 353-363 (2004).
19. Lewis, S.L., *et al*. Increasing carbon storage in intact African tropical forest. *Nature*, **457**, 1003-U3 (2009).
20. Marengo, J.A., *et al.*The drought of Amazonia in 2005. *Journal of Climate*, **21**, 495-516 (2008).
21. Marengo, J.A., *et al.* The drought of 2010 in the context of historical droughts in the Amazon region, *Geophys. Res. Lett.*, **38**, L12703, doi:10.1029/2011GL047436 (2011).
22. Phillips, O., *et al*. Drought Sensitivity of the Amazon Rainforest. *Science*, 323, 1344-1347 (2009).
23. Lenton, T.M., *et al.* Tipping elements in the Earth's climate system. *Proc. Nat. Acad. Sci.*, **105**, 786-793 (2008).
24. Jones, C. D., & Cox, P.M. On the significance of atmospheric CO_2 growth rate anomalies in 2002–2003.*Geophys. Res. Lett.*, **32**, L14816, doi:10.1029/2005GL023027 (2005).
25. Denman, K.L., Brasseur, G., *et al*. Couplings between changes in the climate system and biogeochemistry. In: *Climate Change 2007: The Physical Science Basis. Contribution of Working Group I to the Fourth Assessment Report of the Intergovernmental Panel on Climate Change* [Solomon, S., D. Qin, M. Manning, Z. Chen, M. Marquis, K.B. Averyt,

M.Tignor and H.L. Miller (eds.)]. Cambridge University Press, Cambridge, United Kingdom and New York, NY, USA (2007).

26. Masarie, K.A. & Tans, P.P. Extension and integration of atmospheric carbon dioxide data into a globally consistent measurement record. *J. Geophys. Res.*, **100**, 11593-11610 (1995).
27. M. Meinshausen*, et al*. The RCP greenhouse gas concentrations and their extension from 1765 to 2500. *Climatic Change*, **109**, 213-241 (2011).
28. Smith, T.M., *et al*. Improvements to NOAA's historical merged land-ocean surface temperature analysis (1880-2006). *J. Climate*, **21**, 2283-2296 (2008).
29. Mercado, L.M., *et al*., 2009. Impact of changes in diffuse radiation on the global land carbon sink. *Nature*, **458**, 1014-1018.

Supplementary Information is linked to the online version of the paper at www.nature.com/nature.

Acknowledgements. The authors acknowledge funding from the NERC NCEO programme (P.M.C. and C.M.L.); the EU Greencycles II project (P.M.C. and P.F.); the EU FP7 "CARBONES" project (D.P. and C.D.J.); the Joint DECC/Defra Met Office Hadley Centre Climate Programme (GA01101) (D.P., B.B.B.B and C.J.); the CEH Science Budget (C.H.) and the Newton Institute programme on "Mathematical and Statistical Approaches to Climate Modelling and Prediction" during which this research was first formulated (P.M.C., B.B.B.B. and C.H.). We also acknowledge the modelling groups that provided results to the Coupled Climate Carbon Cycle Model Intercomparison Project (C_4MIP).

Author Contributions. P.M.C. led the study and drafted the manuscript. D.P. assisted with the statistical analysis, especially the estimation of the observationally-constrained PDF in Figure 3(b). P.F. provided data and guidance on the C_4MIP model ensemble, and B.B.B.B. did likewise for the HadCM3 carbon cycle ensemble. C.H. processed observational climate datasets to produce time-series of tropical-mean temperature anomalies. C.J., P.F. and C.H. have been central to discussions over many years concerning the relationship between the interannual variability and the long-term sensitivity of the land carbon cycle to climate change – on which this study is based. C.M.L. provided invaluable insights on the interpretation of the regression line in Figure 3(a). All co-authors commented-on and provided edits to the original manuscript.

Author Information. Reprints and permissions information is available at www.nature.com/reprints. The authors have no competing financial interests. Correspondence and requests for materials should be addressed to P.M.C. (p.m.cox@exeter.ac.uk)

Table and Figure Captions

Table 1: Changes in atmospheric CO_2, tropical land carbon and tropical near-surface air temperature (30°N-30°S), as simulated by the 9 climate-carbon GCMs analysed in this study. Models A to F are from the C4MIP study[3], which prescribed the SRES A1B CO_2 emissions scenario. For these models the changes are calculated over the period 1960 to 2099. Models G to I are from a land carbon cycle parameter ensemble carried-out with the HadCM3 model[14] These latter runs were only out to 2080, so differences here are for 1960 to 2080. In all cases model runs were carried-out both including and excluding climate effects on the carbon cycle ("Coupled" and "Uncoup." respectively), so that the impacts of climate-carbon cycle feedbacks could be diagnosed.

Figure 1: Projected changes in land carbon storage in the tropics from coupled climate-carbon cycle models. (a) upper and lower estimates from the C4MIP models[3] (A-F in table 1) for uncoupled (black lines) and coupled simulations (red lines); (b) impact of changes in tropical temperature versus impact of changes in atmospheric CO_2, for the C4MIP models (black letters) and three variants of the HadCM3C model[14] (red letters). The black dashed horizontal lines represent the new constraint presented in this study.

Figure 2: Observed relationship between interannual variations in the growth-rate of atmospheric CO_2 and inter-annual variations in the annual mean tropical temperature (30°N-30°S). (a) annual anomalies in CO_2 growth-rate (black) and tropical temperature (red) versus year; (b) sensitivity of CO_2 growth-rate to tropical temperature, with numbers representing the individual years in panel (a) and the red dashed-line showing the best-fit straight-line which has a gradient of 5.1 +/- 0.9 GtC/yr/K . The years in red were not included in this fit as these years directly followed major volcanic perturbations to the climate.

Figure 3: Emergent constraint on the sensitivity of tropical land carbon to climate change. (a) Climate sensitivity of tropical land-carbon (γ_{LT}) versus the sensitivity of the CO_2 growth-rate to tropical temperature, for each of the models shown in Table 1. The red-dotted line shows the best-fit straight-line across the C4MIP models (black letters). The red letters represent a test of this relationship against the three HadCM3C ensemble members. The vertical dot-dashed line indicates the constraint on the observed IAV of the CO_2 growth-rate derived from Figure 2(b). (b) Probability density function (PDF) for the climate sensitivity of tropical land-carbon (γ_{LT}). The black line was derived by applying the IAV constraint to the across-model relationship shown in panel (a). The red line shows the "prior" PDF that arises from assuming that all of the C4MIP models are equally likely to be correct and that they come from a Gaussian distribution.

Methods

1 Choice of Models and Variables

In order to make use of the observed interannual variation in atmospheric CO_2 as a constraint, we need climate-carbon cycle simulations that model CO_2 as a "free" fully prognostic variable. We therefore make use of the C4MIP simulations[3] which used prescribed SRES A1B CO_2 emissions but calculated the global mean atmospheric CO_2 concentration interactively. We have augmented the C4MIP results with free CO_2 runs from a carbon cycle parameter ensemble with carried-out with HadCM3[14]. These HadCM3 runs allow the emergent constraint derived from the C4MIP models to be tested over a wide range of possible future carbon losses from tropical land.

In order to derive an emergent constraint it is of paramount importance that equivalent variables are compared from the models and observations. Therefore since the C4MIP models reported global mean atmospheric CO_2, and mean land plus ocean near-surface temperatures, we compute the same diagnostics from the observational datasets (see point 3. below).

2 Diagnosis of γ_{LT}

The sensitivity of tropical land carbon storage to temperature, γ_{LT}, is calculated as in previous studies[3,13]. Firstly, the sensitivity of tropical land carbon storage to direct CO_2 effects, as given by the parameter β_{LT}, is diagnosed from the uncoupled simulation for each model:

$$\beta_{LT} = \frac{\Delta C_{LT}^{u}}{\Delta C_{a}^{u}}$$

where $\Delta C_{LT}^{u} = C_{LT}^{u}(t_1) - C_{LT}^{u}(t_0)$ is the change in tropical land carbon storage (in GtC), and $\Delta C_{a}^{u} = C_{a}^{u}(t_1) - C_{a}^{u}(t_0)$ is the change in global atmospheric CO_2 concentration in (ppmv), in both cases between time t_0 and time t_1 for the uncoupled simulation (denoted by the superscript "u").

This value of β_{LT} is then used to isolate γ_{LT} from the coupled simulation of each model, using the equation:

$$\gamma_{LT} = \frac{\Delta C_{LT}^{c} - \beta_{LT}\, \Delta C_{a}^{c}}{\Delta T_{T}^{c}}$$

where $\Delta C_{LT}^{c} = C_{LT}^{c}(t_1) - C_{LT}^{c}(t_0)$ is the change in tropical land carbon storage (in GtC), $\Delta C_{a}^{c} = C_{a}^{c}(t_1) - C_{a}^{c}(t_0)$ is the change in global atmospheric CO_2 concentration in (ppmv), and

$\Delta T_T^c = T_T^c(t_1) - T_T^c(t_0)$ is the change in mean tropical (30°N-30°S) temperature (in K), in all cases between time t_0 and time t_1 for the coupled simulation (denoted by the superscript "c").

We define the changes relative to 1960 in all cases (i.e. t_0 = 1960), and use the longest possible common simulation periods over which to diagnose β_{LT} and γ_{LT} for the C4MIP models (t_1 = 2099) and the HadCM3C ensemble members (t_1 = 2080), respectively.

3 Sensitivity of CO_2 Growth-Rate Anomaly to Tropical Temperature Anomaly

The sensitivity of the atmospheric CO_2 growth-rate to tropical temperature is calculated over the period 1960 to 2010 inclusive, for the observations and all models. However, for the observational data, and the HadCM3C simulations - which included volcanoes, we exclude the years (1963, 1964, 1982, 1983, 1991, 1992) which were heavily-influenced by the volcanic eruptions[24] of Mt Agung (in 1963), El Chichon (in 1982), and Pinatubo (in 1991). There were two reasons to remove volcanoes. Firstly, not all the models in our ensembles include the climatic effects of volcanic eruptions. Secondly, volcanoes are believed to impact on the land carbon sink through the effects of diffuse radiation fertilization[29], but these effects are not included in the generation of models considered here. We therefore removed "volcano years" from the observations to maximise consistency between models and observations.

For comparability with the outputs available from the C4MIP models we also use the global CO_2 concentration, and the mean tropical temperature (30°N - 30°S) including both land and ocean points.

As in previous studies[24], the annual CO_2 growth-rate for the n_{th} year, $dC_a/dt\ (t_n)$, is defined as the difference between the annual mean CO_2 concentrations for the n_{th} and $(n-1)_{th}$ years:

$$\frac{dC_a}{dt}(t_n) = C_a(t_n) - C_a(t_{n-1})$$

The CO_2 growth-rate is therefore centred in time at the beginning of year n. In order to align the tropical temperature anomalies we take the associated tropical mean temperature, $\overline{T}_T(t_n)$, to be the mean of the annual mean tropical temperatures for year n and year n-1:

$$\overline{T}_T(t_n) = \frac{T_T(t_n) + T_T(t_{n-1})}{2}$$

For all model and observational time-series, the annual CO_2 growth-rate, dC_a/dt, and the associated mean tropical temperature, $\bar{T}_T$, were de-trended using an 11-year running mean, with the residuals defining the annual anomalies (see Supplementary Material, Figure S2). In each case a least-squares linear regression was found between these anomalies in the CO_2 growth-rate and the anomalies in the tropical temperature, with the gradient of the best-fit defining the IAV Sensitivity (see point 5. below).

The IAV sensitivity was calculated for a range of datasets of tropical temperature and atmospheric CO_2 (see point 4. below), so as to explore the uncertainty in the estimate of the IAV sensitivity arising from uncertainties in the observational data. These different estimates are listed in Supplementary Material, Table S1.

In order to isolate the separate contributions of the tropical Net Primary Productivity (NPP) and Soil Respiration, similar regressions against tropical temperature anomalies were carried out separately for each of these fluxes as diagnosed from the C4MIP models (see Suppl. Mat., Figure S1). This showed that the IAV sensitivity across the model ensemble is correlated with the response of tropical Soil Respiration (Figure S1(b)), rather than NPP (Figure S1(c)). By contrast, the wide-range of longer-term projections of changes in land carbon storage is known to be in large part due to the different responses of NPP to climate change[3].

4 Observational Data

Observed annual global CO_2 concentration[26] for 1980 to 2010 was downloaded from the NOAA website (http://www.esrl.noaa.gov/gmd/ccgg/trends/global.html#global_data).

Since this dataset only covers the period from 1980, global CO_2 concentrations for 1960 to 1979 were taken from the historical datasets derived for use with the RCP scenarios[27] (http://www.pik-potsdam.de/~mmalte/rcps/index.htm#).

Tropical (30^{o}N-30^{o}S) annual mean temperatures were calculated from NCDC data[28] (http://www.ncdc.noaa.gov/ghcnm/maps.php), and also from the CRU/Met Office HadCRU3 dataset (http://www.metoffice.gov.uk/hadobs/hadcrut3/), and the GISS dataset (http://data.giss.nasa.gov/gistemp/).

5 Least Squares Linear Regression

Least Squares linear regressions were calculated based on well-established formulae (see for example http://mathworld.wolfram.com/LeastSquaresFitting.html). The linear regression, f_n, between a time-series given by y_n and a time-series given by x_n is defined by a gradient b and intercept a:

$$f_n = a + b\,x_n$$

Minimising the least squares error for y_n involves minimising:

$$s^2 = \frac{1}{N-2}\sum_{n=1}^{N}\{y_n - f_n\}^2$$

where N is the number of data points in each time-series. In this case the best-fit gradient is given by:

$$\bar{b} = \frac{\sigma_{xy}^2}{\sigma_x^2}$$

Here $\sigma_x^2 = \sum_{n=1}^{N}\{x_n - \bar{x}\}^2/N$ is the variance of x_n, and $\sigma_{xy}^2 = \sum_{n=1}^{N}\{x_n - \bar{x}\}\{y_n - \bar{y}\}/N$ is the covariance of the x_n *and* y_n time-series - with means of $\bar{x}$ and $\bar{y}$ respectively.

The standard error of b is given by:

$$\sigma_b = \frac{s}{\sigma_x\sqrt{N}}$$

which defines a Gaussian Probability Density for b:

$$P(b) = \frac{1}{\sqrt{2\pi\sigma_b^2}}\,exp\left\{-\frac{(b-\bar{b})^2}{2\sigma_b}\right\}$$

Finally the "Prediction Error" of the regression is the following function of x:

$$\sigma_f(x) = s\sqrt{1 + \frac{1}{N} + \frac{\{x-\bar{x}\}^2}{N\sigma_x^2}}$$

This expression defines contours of equal probability density around the best-fit linear regression, that represent the probability density of y given x:

$$P\{y|x\} = \frac{1}{\sqrt{2\pi\sigma_f^2}}\,exp\left\{-\frac{(y-f(x))^2}{2\sigma_f}\right\}$$

where $\sigma_f = \sigma_f(x)$, as above.

6 Calculation of Probability Density Function for γ_{LT}

The emergent constraint derived in this study is a linear regression across the C4MIP GCMs between the temperature sensitivity of land carbon storage in the tropics, γ_{LT}, and the sensitivity of the annual growth-rate in atmospheric CO_2 to the annual tropical temperature anomaly, which we label here as γ_{CO2}. In the context of the least squares linear regression presented above, γ_{LT} is equivalent to y, and γ_{CO2} is equivalent to x.

The linear regression therefore provides an equation for the probability of γ_{LT} given γ_{CO2} (i.e. the equation for $P\{y|x\}$ above). Figure S3 (Supplementary Material) shows the best-fit straight-line (thick dashed red line), and the plus and minus σ_f prediction error contours (as thin dashed red lines) on the same scales as Figure 3a.

In addition, the linear regression between the observed annual anomalies in the atmospheric CO_2 growth-rate[25,26] and the tropical mean temperature[27] provides an observation-based PDF for γ_{CO2} (via the equation for $P(b)$ above). The best-fit γ_{CO2} from these observations is shown by the thick dashed vertical line in Figure S3, and the uncertainty in this fit is shown by the thin dashed vertical lines representing plus and minus one standard error about this most likely value.

Given these two PDFs, $P\{\gamma_{LT}|\gamma_{CO2}\}$ and $P(\gamma_{CO2})$, the PDF for γ_{LT} is :

$$P(\gamma_{LT}) = \int_{-\infty}^{\infty} P\{\gamma_{LT}|\gamma_{CO2}\}\, P(\gamma_{CO2})\, d\gamma_{CO2}$$

The integrand $P\{\gamma_{LT}|\gamma_{CO2}\}\, P(\gamma_{CO2})$ is shown by the continuous black contours in Figure S3, and the integral is the basis for the black PDF for γ_{LT} shown in Figure 3b.

		Change in Global Atmospheric CO_2 (ppmv)		Change in Tropical Land Carbon (GtC)		Change in Tropical Temperature (K)
	Model	**Coupled**	**Uncoup.**	**Coupled**	**Uncoup.**	
A	HadCM3LC	689	477	-11	354	3.93
B	IPSL	453	381	177	365	2.70
C	MPI	524	443	242	413	4.36
D	CCSM1	483	465	319	364	1.53
E	FRCGC	589	465	118	271	3.61
F	LOOP	489	460	185	263	3.30
G	HadCM3C-st	599	331	-148	317	4.41
H	HadCM3C-a	445	333	-6	168	3.76
I	HadCM3C-h	589	246	-165	251	4.08

Table 1: Changes in atmospheric CO_2, tropical land carbon and tropical near-surface air temperature (30°N-30°S), as simulated by the 9 climate-carbon GCMs analysed in this study. Models A to F are from the C^{4}MIP study[3], which prescribed the SRES A2 CO_2 emissions scenario. For these models the changes are calculated over the period 1960 to 2099. Models G to I are from a land carbon cycle parameter ensemble carried-out with the HadCM3 model[14]. These latter runs were only out to 2080, so differences here are for 1960 to 2080. In all cases model runs were carried-out both including and excluding climate effects on the carbon cycle ("Coupled" and "Uncoup." respectively), so that the impacts of climate-carbon cycle feedbacks could be diagnosed.

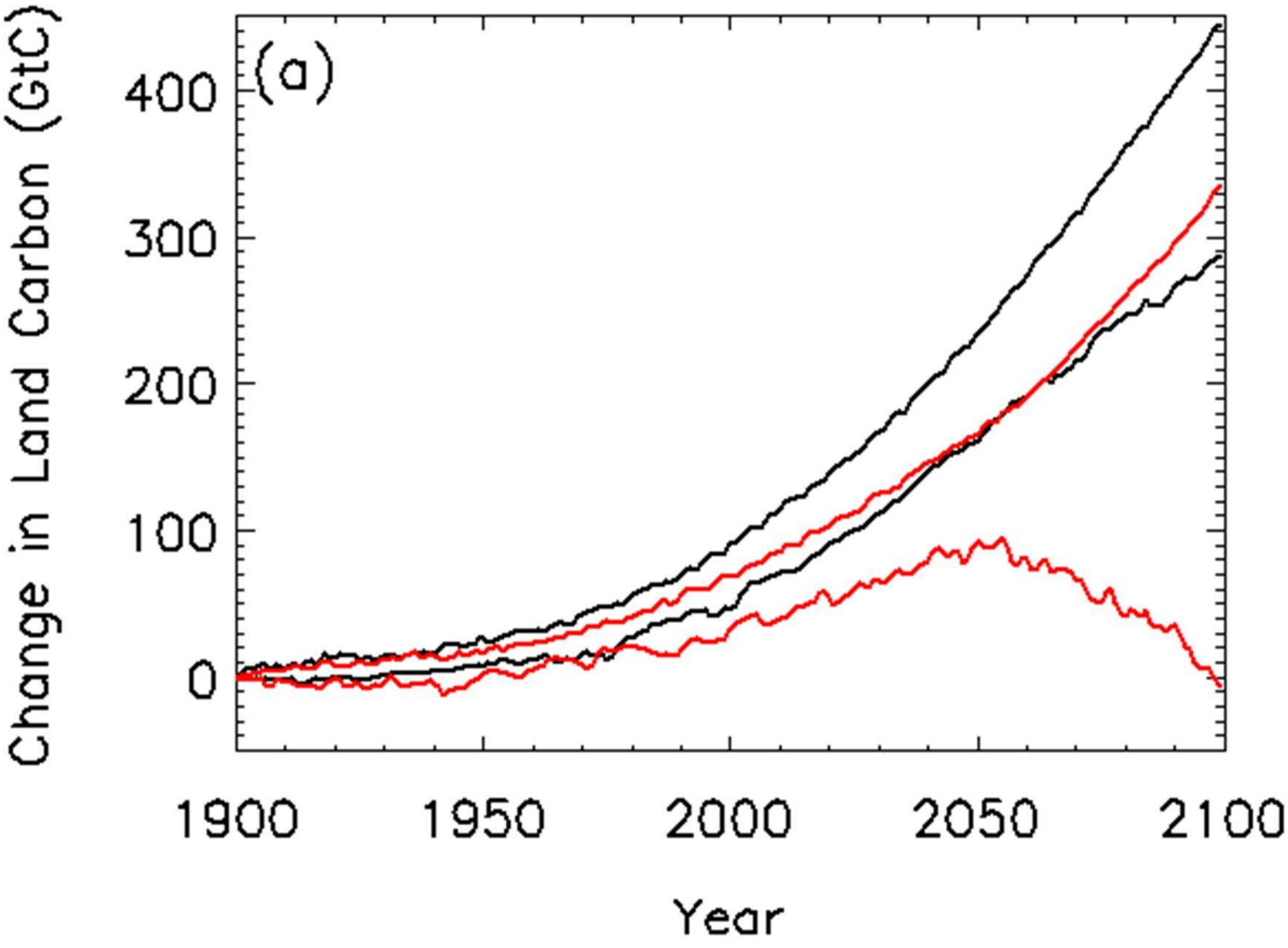
(a)
400
300
200
100
0
Change in Land Carbon (GtC)
1900
1950
2000
2050
2100
Year

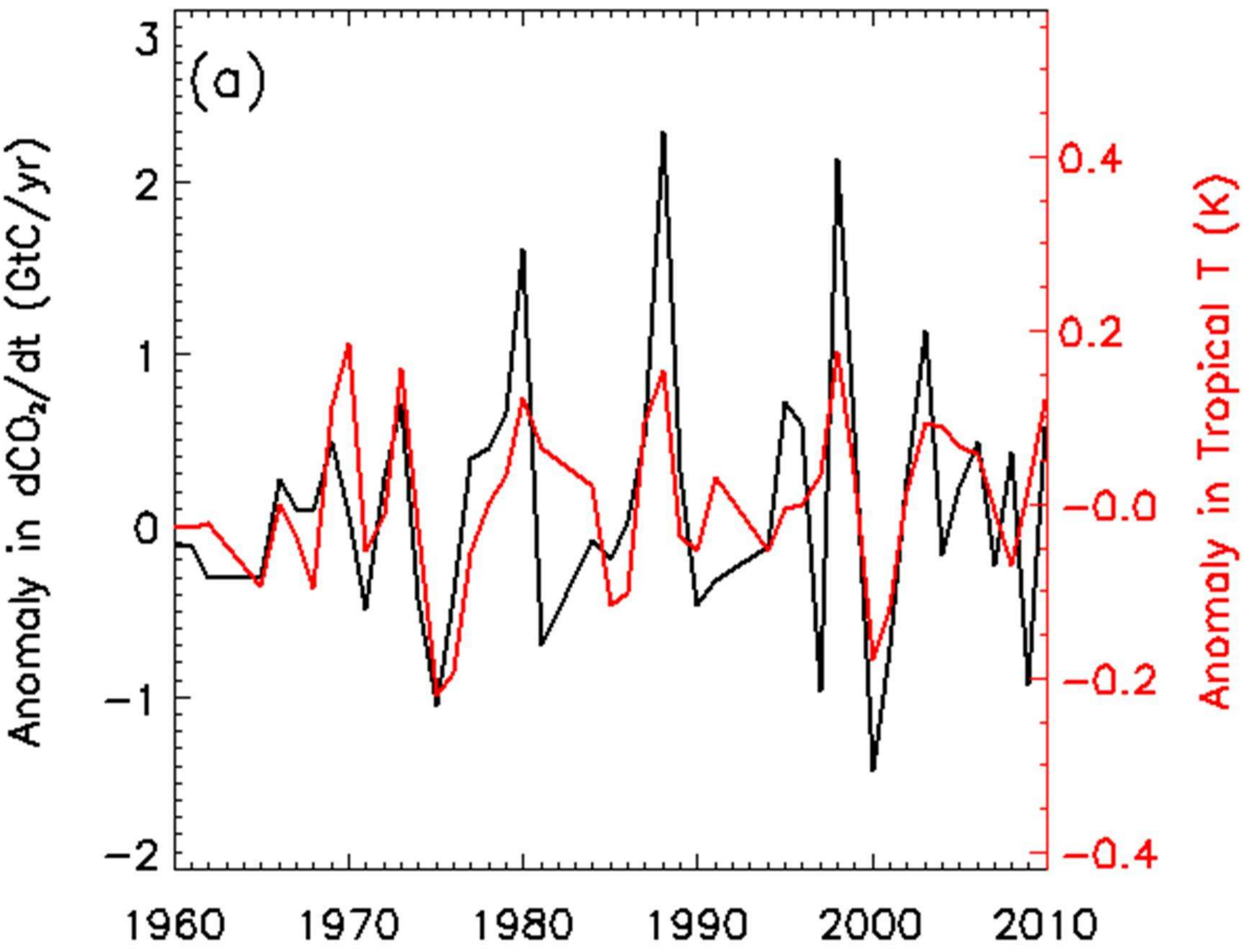
(a)
Anomaly in dCO₂/dt (GtC/yr)
Anomaly in Tropical T (K)
3
2
1
0
−1
−2
0.4
0.2
−0.0
−0.2
−0.4
1960
1970
1980
1990
2000
2010

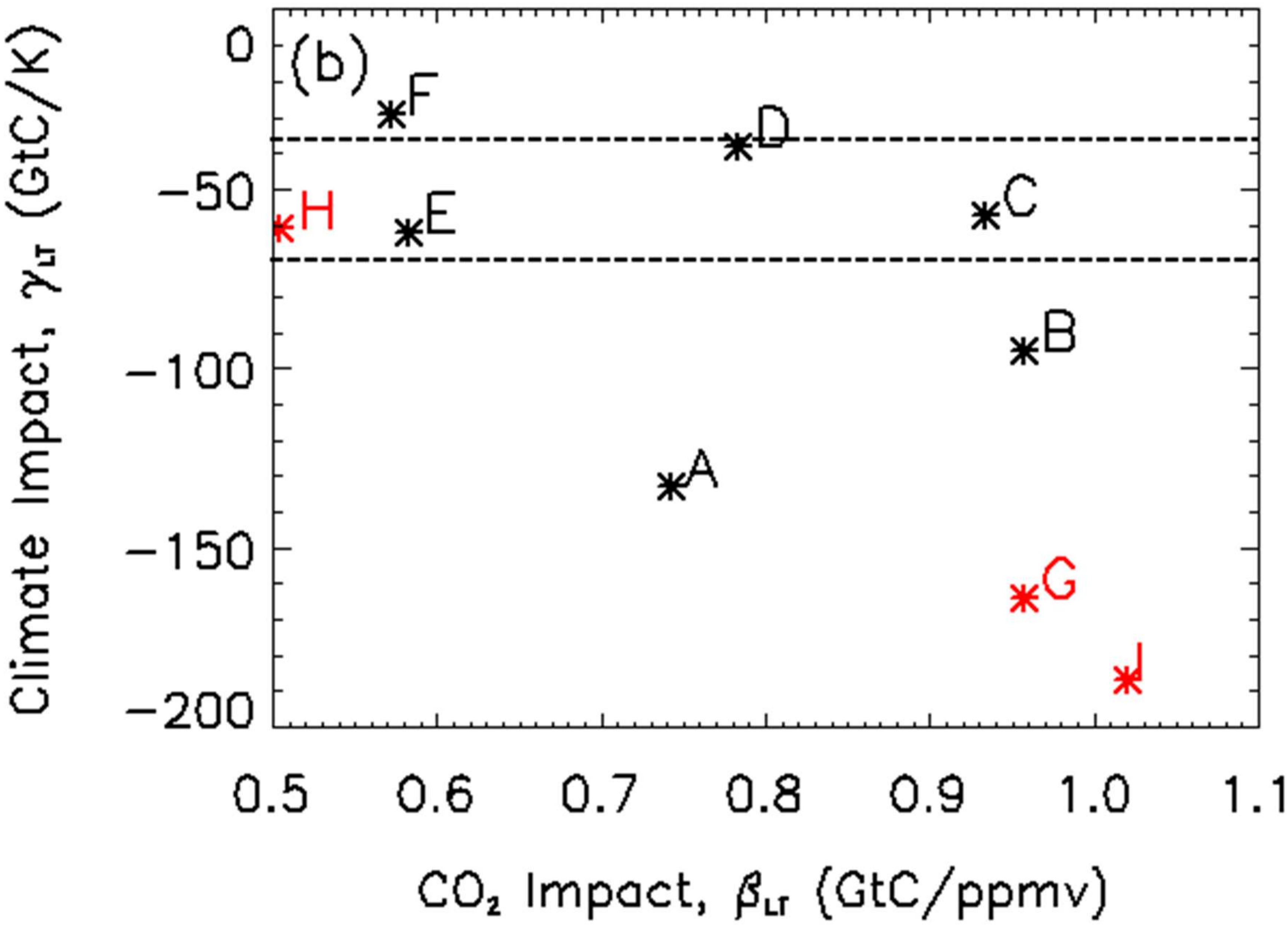

(b)
F
D
C
H
E
B
A
G
I
0
−50
−100
−150
−200
0.5
0.6
0.7
0.8
0.9
1.0
1.1
Climate Impact, γ_{LT} (GtC/K)
CO_2 Impact, β_{LT} (GtC/ppmv)

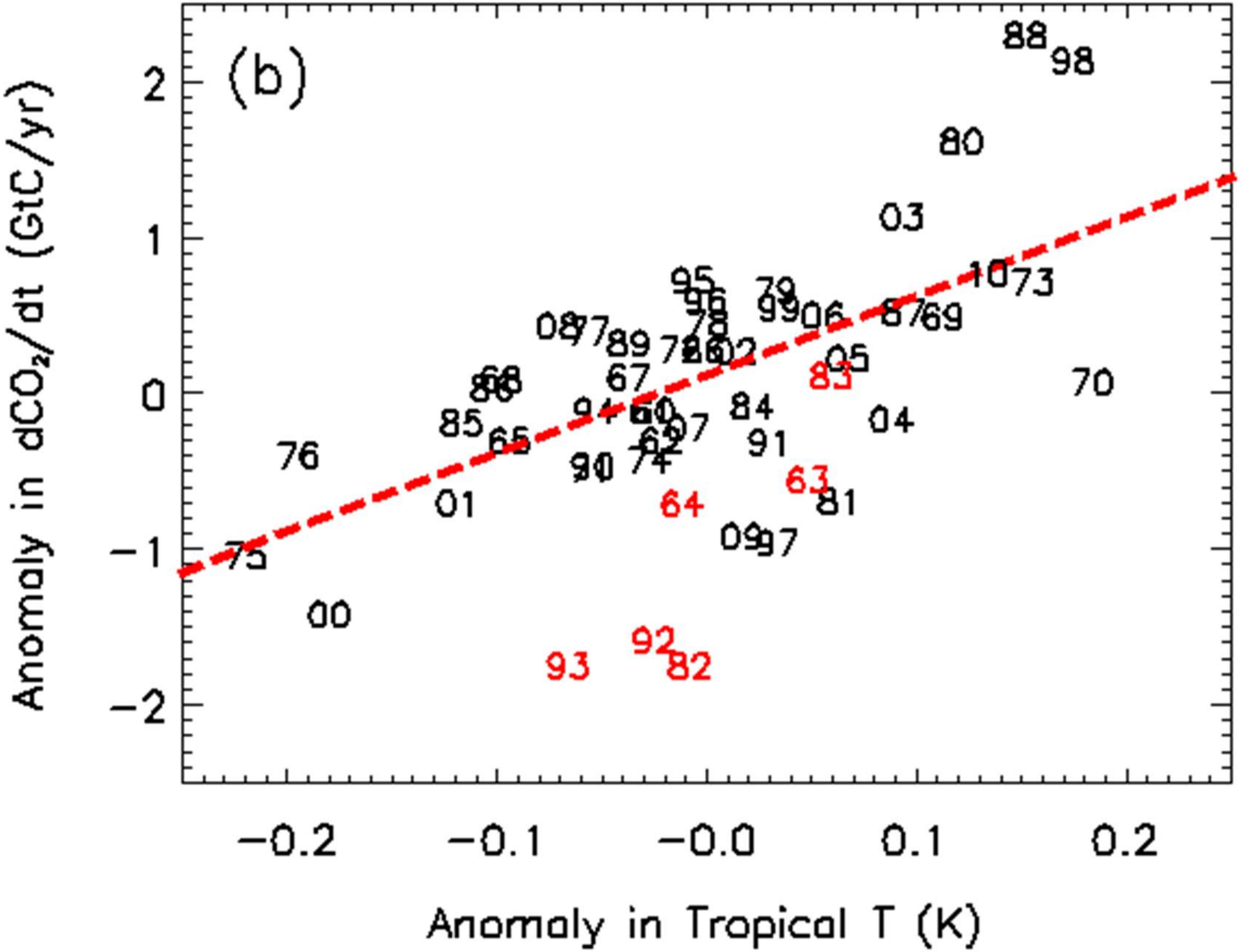
(b)
Anomaly in dCO_2/dt (GtC/yr)
Anomaly in Tropical T (K)
2
1
0
−1
−2
−0.2
−0.1
−0.0
0.1
0.2

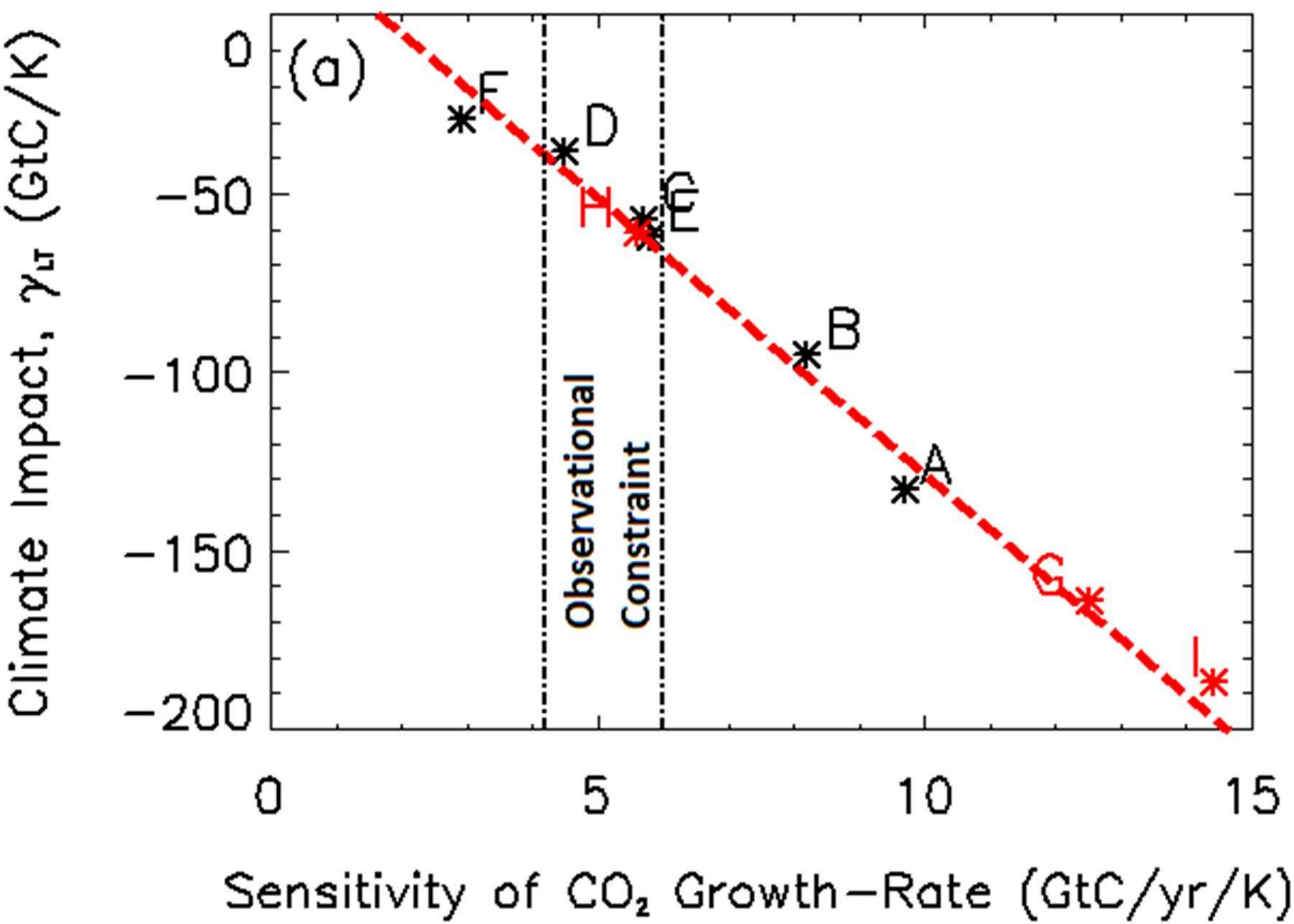

(a)
F
D
C
E
H
B
A
G
I
Observational
Constraint
0
-50
-100
-150
-200
0
5
10
15
Climate Impact, γ_{LT} (GtC/K)
Sensitivity of CO_2 Growth-Rate (GtC/yr/K)

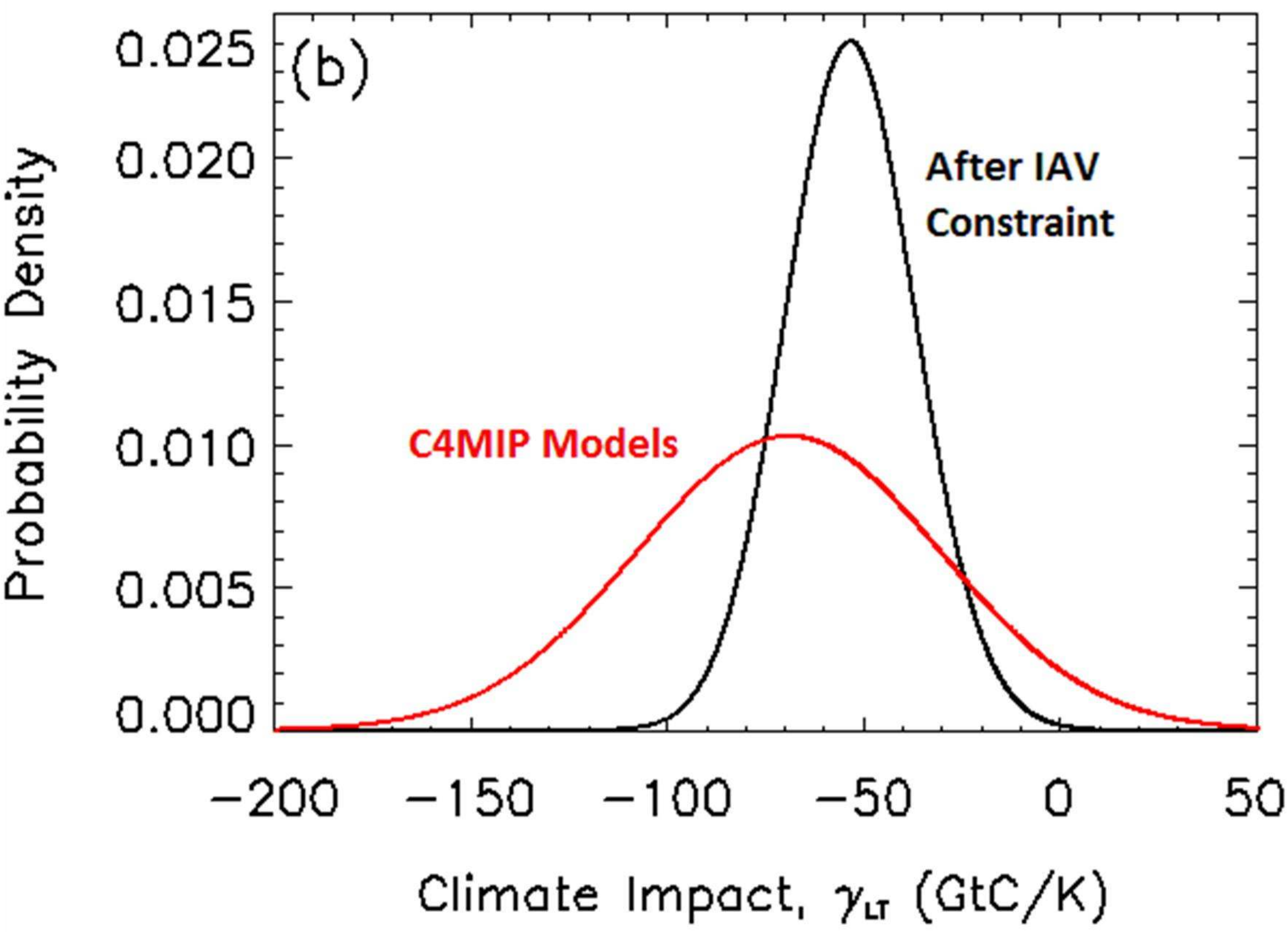

(b)
After IAV
Constraint
C4MIP Models
Probability Density
0.025
0.020
0.015
0.010
0.005
0.000
−200
−150
−100
−50
0
50
Climate Impact, γ_{LT} (GtC/K)